Acta Pharmaceutica Sinica B 2018;8(5):825–832

Chinese Pharmaceutical Association
Institute of Materia Medica, Chinese Academy of Medical Sciences

Acta Pharmaceutica Sinica B

www.elsevier.com/locate/apsb
www.sciencedirect.com

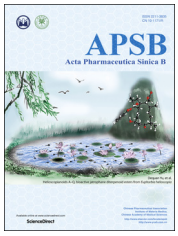

ORIGINAL ARTICLE

Efficacy of inverso isomer of CendR peptide on tumor tissue penetration

Ruifeng Wang[†], **Qing Shen**[†], **Xue Li, Cao Xie, Weiyue Lu, Songli Wang, Jing Wang, Dongli Wang, Min Liu**[*]

Key Laboratory of Smart Drug Delivery, Ministry of Education, Department of Pharmaceutics, School of Pharmacy, Fudan University, Shanghai 201203, China

Received 29 January 2018; received in revised form 16 April 2018; accepted 26 April 2018

KEY WORDS

Inverso isomer;
CendR peptide;
Neuropilin-1 (NRP-1);
Tumor penetration;
Gemcitabine

Abstract The dense extracellular matrix and high interstitial fluid pressure of tumor tissues prevent the ability of anti-tumor agents to penetrate deep into the tumor parenchyma for treatment effects. C-end rule (CendR) peptides can enhance the permeability of tumor blood vessels and tumor tissues *via* binding to neuropilin-1 (NRP-1), thus aiding in drug delivery. In this study, we selected one of the CendR peptides (sequence RGERPPR) as the parent L-peptide and substituted D-amino acids for the L-amino acids to synthesize its inverso peptide $_{D}$(RGERPPR). We investigated the NRP-1 binding activity and tumor-penetrating ability of $_{D}$(RGERPPR). We found that the binding affinity of $_{D}$(RGERPPR) with NRP-1 and the cellular uptake was significantly higher than that of RGERPPR. Evans Blue tests revealed that $_{D}$(RGERPPR) exhibited improved tumor-penetrating ability in C6, U87 and A549 tumor-bearing nude mice. Using nude mice bearing A549 xenograft tumors as a model, we found that the rate of tumor growth in the group co-administered with $_{D}$(RGERPPR) and gemcitabine (Gem) was significantly lower than the gemcitabine-treated group with a tumor suppression rate (TSR%) of 55.4%. Together, our results demonstrate that $_{D}$(RGERPPR) is a potential tumor-penetrating peptide.

[*]Corresponding author.
E-mail address: liumin@shmu.edu.cn (Min Liu).
[†]These authors contributed equally to this work as co-first authors.

Peer review under responsibility of Institute of Materia Medica, Chinese Academy of Medical Sciences and Chinese Pharmaceutical Association.

https://doi.org/10.1016/j.apsb.2018.06.006

1. Introduction

Tumor tissues exhibit specific pathological features, including large amounts of random vasculature with high permeability, the absence of lymphatic drainage, a dense extracellular matrix, high interstitial fluid pressure, and an acidic and anoxic environment in the center of the tumor that is caused by poor elimination of metabolites owing to insufficient blood supply[1–8]. Because of the dense extracellular matrix and high interstitial fluid pressure, antitumor agents are unable to reach deep into the tumor parenchyma, leading to retention of drugs around the tumor blood vessels. This non-uniform distribution of drugs is one of the crucial reasons for relapse and metastasis, which is serious obstacle in the treatment of tumors.

Neuropilin-1 (NRP-1), a transmembrane glycoprotein, was first discovered in the nervous system of *Xenopus tadpoles* by Takagi et al.[9] *via* hybridoma technology in 1987. As a coreceptor of sema3A and VEGF165, NRP-1 played an important role in tumor occurrence, growth, and metastasis[10–12]. NRP-1 was highly expressed on many tumor cells including glioma, non-small cell lung cancer, pancreatic cancer, gastric cancer, colon cancer and breast cancer[13–15]. A series of peptides possessing a consensus R/KXXR/K motif with L-amino acids were identified that showed high binding affinity to NRP-1[13]. The C-terminal arginine (or rarely lysine) was important for NRP-1 binding activity. Adding another amino acid or blocking the free carboxyl group of this arginine residue by amidation eliminated the binding activity to NRP-1. This strict requirement for a C-terminal residue was termed as the C-end rule (CendR). By binding NRP-1, the CendR peptides could induce enhanced permeability of tumor blood vessels and tumor tissues, which could enhance the tissue-penetrating ability of free drugs and nanodrug delivery systems.

Despite these initial promising results, these linear L-peptides are susceptible to protease degradation in plasma and readily lose their bioactivity. In our previous study, we selected one of CendR peptides (sequence RGERPPR) as a parent L-peptide and synthesized its retro-inverso isomer, $_{D}$(RPPREGR)[16,17]. The retro-inverso peptide was composed of D-amino acids assembled in the reverse order from that in the parent L-sequence[18]. Compared with RGERPPR, $_{D}$(RPPREGR) not only showed improved biological stability but also increased binding affinity to NRP-1. We synthesized $_{D}$(RPPREGR) modified highly branched polyethyleneimine as gene vector, which significantly enhanced the therapeutic effect of genes on orthotopic tumor-bearing animal models.

The inverso peptide, which is composed of D-amino acids assembled in the same order as that in the parent L-sequence, shows a mirror-image relationship with the parent L-peptide. In general, the inverso peptide might not have similar bioactivity as its parent L-peptide. However, CendR peptides are a series of specific peptides with a consensus R/KXXR/K motif and exhibited high binding affinity to NRP-1 and improved tumor-penetrating ability. The inverso isomer of CendR peptides also has a consensus $_{D}$(R/KXXR/K) motif. Since the C-terminal amino acid of the inverso isomer is arginine or lysine, we speculate that the inverso isomer of CendR peptides also have NRP-1 binding activity and tumor-penetrating ability. To verify our hypothesis, in this paper, we chose RGERPPR as the parent L-peptide and synthesized its inverso isomer, $_{D}$(RGERPPR). We then investigated the activities of $_{D}$(RGERPPR), including binding affinity to NRP-1, tumor cell internalization and tumor-penetrating ability.

2. Methods

2.1. Materials

Boc-protected amino acid was purchased from Peptide International (Japan). Hydrogen amine resin and 4-methylbenzene was supplied by Bachem AG (Switzerland). Diisopropylethylamine (DIEA) was obtained from Fluka (USA). *O*-(Benzotriazol-1-yl)-*N*,*N*,*N*′,*N*′-tetramethyluronium hexafluorophosphate (HBTU) was from American Bioanalytical (USA). iRGD (CRGDKGPDC) was purchased from ChinaPeptides (Shanghai, China). Fluorescein-5-maleimide (Mal-FITC) was purchased from Fanbo Biochemicals (Beijing, China). Phosphate-buffered saline (PBS), plastic cell culture dishes and plates were supplied by Corning Incorporated (Corning, USA). Dulbecco's modified Eagle's medium (DMEM), fetal bovine serum (FBS), trypsin-EDTA (0.25%) and penicillin–streptomycin were from Gibco (Life Technology, USA). Evans Blue was purchased from Ourchem (Shanghai, China). Gemcitabine hydrochloride and carboplatin were obtained from Meilun Biological Technology Co. Ltd. (Dalian, China). Thiazolyl blue tetrazolium bromide (MTT) and all other chemical reagents were analytical pure grade and obtained from Sigma–Aldrich (St Louis, MO, USA).

2.2. Synthesis of peptides and FITC-labeled peptides

RGERPPR, $_{D}$(RPPREGR), $_{D}$(RGERPPR), CRGERPPR, $_{D}$(CRPPREGR) and $_{D}$(CRGERPPR) were synthesized using Boc-protected solid phase peptide synthesis strategy on 4-methylbenzene and hydrogen amine resin. Resin was swelled with *N*,*N*-dimethylformamide for 20 min. The Boc-protected amino acid was activated by dissolving in HBTU and DIEA for 2 min. The activated amino acid solution was then added to the resin and mixed by stirring for 20 min. The amino group was deprotected by approximately twice the resin volume of trifluoroacetic acid and reacted with the carboxyl group of the next Boc-protected amino acid. This cycle was repeated to form the desired peptide chain. The peptide was then cut from resin by hydrogen fluoride. To prepare fluorescein-labeled peptides and decrease the interference of fluorescein, the N-terminals of RGERPPR, $_{D}$(RPPREGR) and $_{D}$(RGERPPR) were extended with cysteine. After purification to homogeneity *via* high-performance liquid chromatography (HPLC), all synthetic peptides were analyzed by ultraperformance liquid chromatography (UPLC) and electrospray ionization-mass spectrometry (ESI-MS). RGERPPR, $_{D}$(RPPREGR), and $_{D}$(RGERPPR) were also characterized by circular dichroism spectrum.

To synthesize FITC-CRGERPPR, a 1.2 × molar excess of Mal-FITC was dissolved in 1 mL of PBS with 5 mg CRGERPPR and stirred for 1 h in the dark. The reaction solution was purified *via* HPLC. The syntheses of other FITC-labeled peptides were the same as described for FITC-CRGERPPR. All FITC-labeled peptides were analyzed by UPLC and ESI-MS.

2.3. Surface plasmon resonance studies

To evaluate the binding affinity of RGERPPR, $_{D}$(RPPREGR) and $_{D}$(RGERPPR) with NRP-1, SPR interaction analyses were conducted using a Biacore T200 system (GE Healthcare, Uppsala, Sweden). First, the NRP-1 protein was coupled to the CM5 sensor chip *via* the standard amine coupling procedure. The peptides were then dissolved in HBS-EP (pH 4.0) buffer from low to high concentration (31.25 nmol/L to 1 μmol/L) and injected for detect-

ing resonance changes. Data were analyzed by Biacore T200 evaluation software (GE Healthcare).

2.4. Computer-aided simulated design

The crystal structure model of NRP-1 protein was downloaded from www.pdb.org (pdb code: 5j1x). The missing atoms in the protein structure were added by the protein prepare package in the software Schrodinger Suites (2015, Schrödinger, LLC, New York, USA). The structure model of CendR peptides was built with the software Schrodinger and optimized in OPLS2005 force field. The design peptides were docked to NRP-1 protein by the Glide package in Schrodinger with default parameters[19–22]. The binding energy was predicted by Glide. The resulting binding modes were analyzed, and the figures presented in paper were made by the software PyMOL (Version 1.3, Schrödinger, LLC, New York, USA).

2.5. Cell culture

Human lung adenocarcinoma epithelial cells (A549), human umbilical vein endothelial cells (HUVEC), human glioblastoma-astrocytoma cells (U87), and C6 rat malignant glioma cells were obtained from the Shanghai Institute of Cell Biology. Cells were cultured in DMEM containing 10% FBS, 100 U/mL penicillin and 100 mg/mL streptomycin at 37 °C under 5% CO_2 atmosphere.

2.6. Cellular uptake and flow cytometry tests

HUVECs were seeded in 12-well plates at a density of 8×10^4 cells/well in 1 mL of DMEM with 10% FBS and incubated overnight (5% CO_2) at 37 °C. FITC-CRGERPPR, FITC-$_D$(CRPPREGR) and FITC-$_D$(CRGERPPR) were added to the plates at a final concentration of 5×10^{-6} mol/L and incubated for 4 h. HUVECs were washed with PBS (0.01 mol/L, pH 7.4) twice and fixed with 10% formaldehyde for 10 min. The cells were washed with PBS twice and then overlaid with 10% buffered glycerol saline before observation using an inverted fluorescence microscope (Leica, DMI4000B, Wetzlar, Germany).

For flow cytometry evaluation, following the incubation described above, the HUVECs were trypsinized, centrifuged, resuspended in 300 μL PBS and analyzed by flow cytometry (FACSAria, BD, USA). Cellular uptake and flow cytometry tests of C6 cells, U87 cells and A549 cells were performed as the same as described for HUVECs.

2.7. Cytotoxicity assay

A549 cells were seeded into 96-well plates (5×10^3 cells/well) with 200 μL/well DMEM containing 10% FBS, 100 U/mL penicillin and 100 mg/mL streptomycin and incubated at 37 °C, 5% CO_2 for 24 h. Various concentrations of gemcitabine or carboplatin in PBS were added into the wells, and plates were incubated at 37 °C, 5% CO_2 for 48 h. Control cells were treated with fresh medium. Twenty microliters of 5 mg/mL MTT solution was added to each well and plates were incubated for 4 h. The medium was then removed, and 150 μL of DMSO was added to dissolve the formazan crystals. After 15 min, measurements were performed using a microplate reader (wavelength, 490 nm; PowerWave XS, Bio-TEK, Winooski, VT, USA). The measurements for each sample were conducted in triplicate.

2.8. Animal model establishment

Male nude mice (6–8 weeks old, 18–22 g weight) were purchased from Shanghai Sippr-BK Laboratory Animal Co. Ltd. (Shanghai, China). Mice were kept under specific pathogen-free conditions and provided with sufficient food and water. All animal experiments were conducted in accordance with the guidelines evaluated and approved by the Ethics Committee of Fudan University. The tumor model was established by subcutaneous injection of A549 cells (7×10^6 cells), C6 cells (8×10^6 cells) or U87 cells (9×10^6 cells) in 100 μL PBS into the right flank region of nude mice.

2.9. Tumor-penetrating ability study

The C6, U87, and A549 tumor-bearing nude mice were intravenously injected with 1 mg of Evans blue in PBS, followed another injection 5 min later with 4 μmol/kg of $_D$(RGERPPR) or iRGD in PBS. The control mice were treated with an equal volume of PBS. The animals were perfused through the heart with PBS 30 min later, and then tumor tissues were collected and cut into pieces. Evans blue was extracted by incubating the tissue pieces in *N*,*N*-dimethylformamide at 37 °C in a water-bath shaker kept for up to 24 h. After centrifugation (4000 rpm, 10 min, Centrifuge H1650-W, Xiangyi, Changsha, China), the absorbance of the supernatant was measured *via* an ultraviolet spectrophotometer at 600 nm.

2.10. In vivo treatment study

The A549 tumor-bearing nude mice were randomly divided into four treatment groups ($n = 5$) when the tumors reached an average volume of 170 mm^3. Mice were injected intravenously *via* a tail vein twice a week for a total of 5 times with the following: 1) equal volume of PBS (the control group); 2) $_D$(RGERPPR) (total dose 20 μmol/kg) in PBS; 3) the free form of gemcitabine (total dose 75 mg/kg) dissolved in PBS; 4) gemcitabine (total dose 75 mg/kg) in PBS combined with $_D$(RGERPPR) (total dose 20 μmol/kg) in PBS. Every two days, tumor size was measured across its two perpendicular diameters using a vernier caliper. The volume (V) was calculated according to formula

$$V = 0.5 \times a \times b^2 \quad (1)$$

where a and b are the longest and shortest diameters of the tumors, respectively. Tumor suppression rate was calculated as follows:

$$\mathrm{TSR}\% = \left[(V_c - V_t)/V_c\right] \times 100 \quad (2)$$

where V_c is the tumor volume of the control group and V_t is the tumor volume of the treatment group.

2.11. Statistical analysis

All data are represented as mean ± SEM for all quantitative data. Statistical analysis was performed with the GraphPad Prism software. Two-tailed Student's *t*-test was used to determine significant differences between two groups ($^*P < 0.05$). Two-way analysis of variance (ANOVA) was used to determine significant differences between multiple groups ($^*P < 0.05$, $^{****}P < 0.0001$). ns indicates no significant differences ($P > 0.05$).

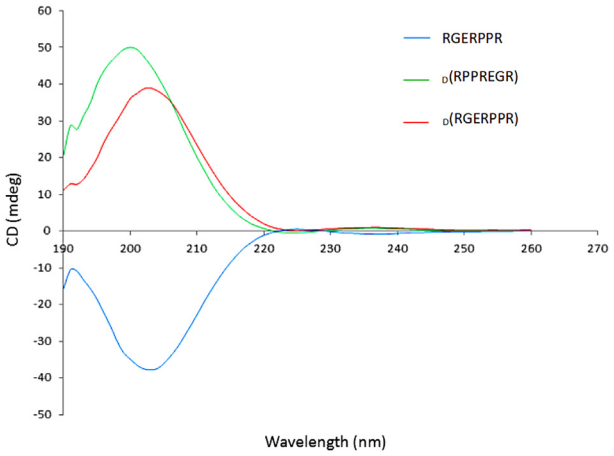

Figure 1 Circular dichroism spectrum of RGERPPR, D(RPPREGR) and D(RGERPPR). The peptides were dissolved in deionized water at a concentration of 0.5 mg/mL for detection.

3. Results

3.1. Characterization and evaluation of peptides

Using a solid phase peptide synthesis strategy, we successfully obtained adequate quantities of highly pure RGERPPR, D(RPPREGR), D(RGERPPR) and FITC-labeled peptides. The HPLC and ESI-MS data (Supplementary Information Fig. S1) confirmed high purity levels and the molecular weight fit the theoretical value. RGERPPR, D(RPPREGR) and D(RGERPPR) were also characterized by circular dichroism spectrum (Fig. 1). All three peptides had an absorption peak at about 200 nm, indicating that the three peptides are disordered linear peptides. Moreover, the absorption peak of D(RGERPPR) was enantiomorphous with RGERPPR, indicating that the optical rotation of D(RGERPPR) was opposite to RGERPPR, proving that the peptides had different configurations. To evaluate the binding affinity of peptides to the NRP-1, we conducted SPR interaction analyses using a Biacore T200 optical biosensor. The D(RGERPPR) peptide registered a K_d value of 44.3 nmol/L, which was approximately 7.7 and 2 times lower than that of RGERPPR and D(RPPREGR), respectively (Table 1 and Supplementary information Fig. S2), indicating D(RGERPPR) possessed higher binding affinity to NRP-1.

3.2. Computational analyses

Here we designed a peptide comprised of D-amino acids, D(RGERPPR). Notably, although the side chain of residues in D(RGERPPR) and D(RPPREGR) adopted opposite orientations compared with the reported active L-peptide, D(RGERPPR) and D(RPPREGR) showed higher binding affinity to the NRP-1. We performed a molecular docking study with the Schrodinger software package to explore the binding modes of the active peptides and determine the reason for the higher binding affinity of the two peptides comprised of D-amino acids. The three peptides were docked into the binding pocket of NRP-1 with the peptide docking package in Schrodinger. Examination of the binding modes of the peptides revealed that RGERPPR adopted the classic binding mode of the C-end peptide, in which the Arg7 at the C-terminal formed an ion interaction with Asp320 in NRP-1, and the COO^- at the C-terminal formed a hydrogen bond network with Tyr353, Ser346, Thr349 and Trp301. Arg1 and Arg4 formed hydrogen bonds with the backbone of NRP-1. Arg7 and Arg1 formed cation–π interactions with Tyr353 and Tyr297 (Fig. 2 A and B).

In the binding mode of D(RPPREGR), the DArg1 at the N-terminal formed an ion interaction with Glu319 in NRP-1, and the NH_3^+ at the N-terminal interacted with Asp320. DArg4 formed a cation–π interaction with Tyr297 and Tyr353. DArg7 formed an ion interaction with Glu348 (Fig. 2C and D).

In the binding mode of D(RGERPPR), the three DArg residues also formed a strong hydrogen network and ion interaction with the residues of NRP-1. DArg7 interacted with negatively charged Glu324 and Glu319. DArg4 formed hydrogen bonds with the backbone of NRP-1. DArg1 in D(RGERPPR) formed ion interactions with Asp320. DArg1 and DArg4 also formed cation–π interactions with Tyr353 and Tyr297 (Fig. 2E and F).

In the sequence of the peptides, the Arg or DArg residues contributed to the primary binding affinity of the peptides. Comparing the binding modes of the three peptides, the three DArg residues in D(RGERPPR) and D(RPPREGR) fit well with the binding pocket and effectively interact with residues in NRP-1 by hydrogen bond, ion interaction and cation–π interaction. In the sequence RGERPPR, only Arg7 at the C-terminal could form strong interaction with the residues of NRP-1, and Arg1 and Arg4 formed weak interaction with the backbone of NRP-1. We predicted the binding affinity of the three peptides (Table 1), which indicated that D(RGERPPR) and D(RPPREGR) were more potent than RGERPPR, and D(RGERPPR) was slightly stronger than D(RPPREGR) in terms of binding affinity. The computational predicted result was also in good agreement with SPR-determined results. These results demonstrate that D(RGERPPR) and D(RPPREGR) possessed stronger binding affinity to NRP-1 compared with RGERPPR.

3.3. In vitro cellular uptake of peptides

The cellular uptake and flow cytometry data for FITC-CRGERPPR, FITC-D(CRPPREGR), and FITC-D(CRGERPPR) were shown in Fig. 3. In the cell uptake experiments, higher fluorescent signals of FITC-D(CRGERPPR) were observed in HUVEC, C6, U87 and A549 cells compared with FITC-D(CRPPREGR) and FITC-CRGERPPR. The mean fluorescent intensity of FITC-D(CRGERPPR) in HUVECs was nearly 13.1 times higher than that of FITC-CRGERPPR, and 5.7 times higher than that of FITC-D(CRPPREGR). In C6 and U87 cells, the mean fluorescent intensity of FITC-D(CRGERPPR) was 5.4 times and 3.3 times higher than that of FITC-CRGERPPR, and 2.9 times and 3.5 times higher than FITC-D(CRPPREGR), respectively. FITC-positive

Table 1 Experimentally determined and predicted free energies of binding of the peptides with NRP-1 ($\Delta G = 1.3636 \log K_d$).

Peptide	K_d (nmol/L)	Experimental ΔG (kcal/mol)	Predicted ΔG (kcal/mol)
RGERPPR	580	–8.50	–8.03
D(RPPREGR)	88.5	–9.61	–8.58
D(RGERPPR)	44.3	–10.02	–9.31

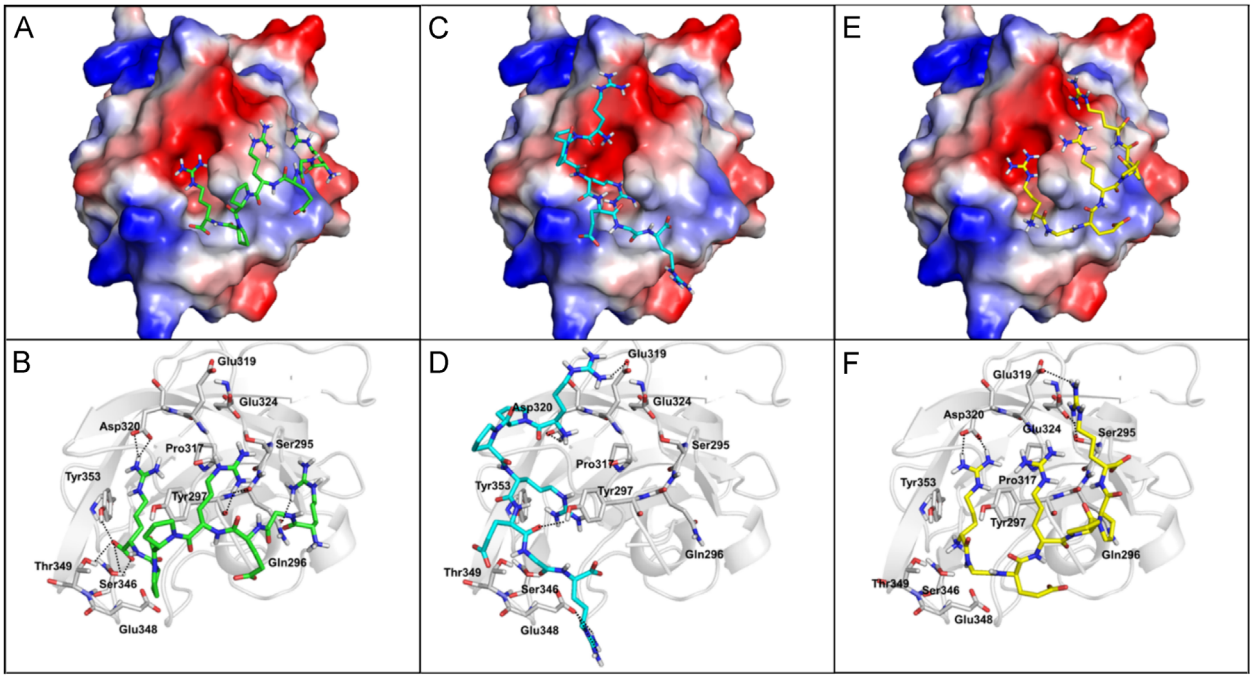

Figure 2 Interaction of CendR peptides with receptors. (A), (C) and (E) NRP-1 is represented by the electrostatic potential surface. The designed peptides are shown in stick models and colored as green, blue and yellow for RGERPPR, D(RPPREGR) and D(RGERPPR), respectively. (B), (D) and (F) NRP-1 is represented by cartoon models. The interacting residues in the binding pocket and the peptides are shown in stick models.

ratio of FITC-$_D$(CRGERPPR) in A549 cells was 1.3 times and 1.6 times higher than that of FITC-$_D$(CRPPREGR) and FITC-CRGERPPR. These data indicated that the cellular uptake efficiencies of $_D$(RGERPPR) by HUVEC, C6, U87 and A549 cells were higher than that of both RGERPPR and $_D$(RPPREGR), which was consistent with the result of SPR interaction analyses above. As HUVECs can simulate tumor neovascularization[23], we speculated that $_D$(RGERPPR) possessed the capacity to target tumor vessels. Thus, $_D$(RGERPPR) might have broad-spectrum tumor-penetrating ability.

3.4. *Tumor-penetrating ability of $_D$(RGERPPR)*

Based on aforementioned investigations *in vitro*, we can conclude that $_D$(RGERPPR) possessed higher NRP-1 binding affinity and better cellular uptake efficiencies than other two peptides. Next, we investigated the tumor-penetrating ability of $_D$(RGERPPR) *in vivo*.

Evans blue is a water-soluble albumin-binding dye, which was used to assess the integrity of blood vessels[24] as well as the tumor-penetrating effect mediated by NRP-1[25]. Sugahara et al.[25] designed a cyclic peptide containing the CendR motif, iRGD (CRGDKGPDC), possessing tumor-penetrating ability. The iRGD peptide was cleaved by protease to expose the cryptic CendR motif: CRGDK. The CendR peptide then mediated binding to NRP-1 resulting enhanced permeability of tumor blood vessels and tumor tissues, which was confirmed *via* quantification of tumor-specific entry of Evans blue into tumor tissues. In this study, $_D$(RGERPPR) co-administrated with the Evans blue dye, caused tumor-specific accumulation of the dye in all 3 tumor models we tested (Fig. 4). Compared with the control PBS group, $_D$(RGERPPR) increased the Evans blue permeation by 36.4%, 30.5% and 46.4% in C6, U87 and A549 subcutaneous tumor models, respectively. By contrast, iRGD increased the Evans blue permeation by 49.7%, 17.7% and 32.9% in C6, U87 and A549 subcutaneous tumor models, respectively. According to a previous report, iRGD could remarkably increase the permeability of tumor tissues[25]. In our research, we found that the tumor-penetrating ability of $_D$(RGERPPR) was comparable to that of iRGD in C6, U87 and A549 tumor-bearing nude mice. Furthermore, the Evans blue average permeation of PBS group in A549 tumor model was 3.04 times and 12.25 times higher than that of C6 tumor model and U87 tumor model, indicating that tumor tissue of A549 tumor model has better permeability. And the tumor-penetrating ability of $_D$(RGERPPR) was the highest in A549 tumor-bearing mice among three tumor models. Based on the above considerations, the *in vivo* treatment study was then performed on the A549 subcutaneous tumor model.

3.5. *In vivo anti-tumor efficiency*

We examined gemcitabine and carboplatin, as these are mainly used as first-line therapy in clinical treatment for non-small-cell lung cancer. The *in vitro* cytotoxicity of gemcitabine and carboplatin were measured by MTT assays. The IC_{50} values were 4.83×10^{-6} mol/L for gemcitabine and 1.38×10^{-4} mol/L for carboplatin after 48 h treatment (Supplementary Information Fig. S3), indicating that gemcitabine exhibited higher growth inhibitory effects in A549 cells than carboplatin.

The *in vivo* antitumor efficiency was next investigated on nude mice bearing A549 cell-derived xenograft tumors. PBS, $_D$(RGERPPR), gemcitabine, or gemcitabine combined with $_D$(RGERPPR) were injected *via* the tail vein. To evaluate tumor growth, tumor volumes (V_n) were divided by their primary tumor volume (V_0) (Fig. 5). Compared with the PBS treatment group, the gemcitabine combined with $_D$(RGERPPR) treatment was effective

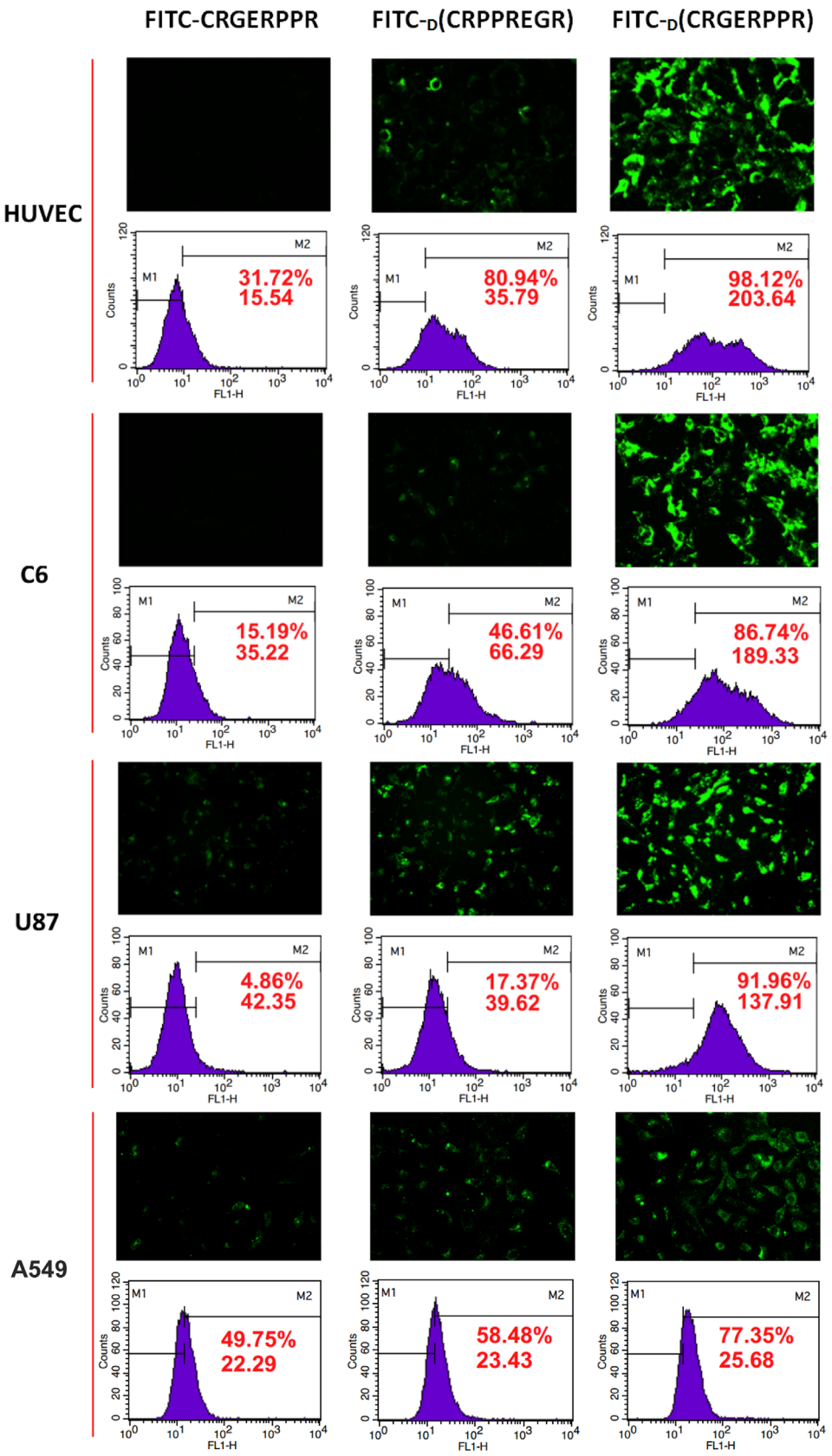

Figure 3 Representative images of cellular uptake and flow cytometry data for FITC-CRGERPPR, FITC-D(CRPPREGR), and FITC-D (CRGERPPR) in various cell lines as indicated. Percentages and numbers below in the flow cytometry data represent FITC-positive ratios and mean fluorescent intensities, respectively.

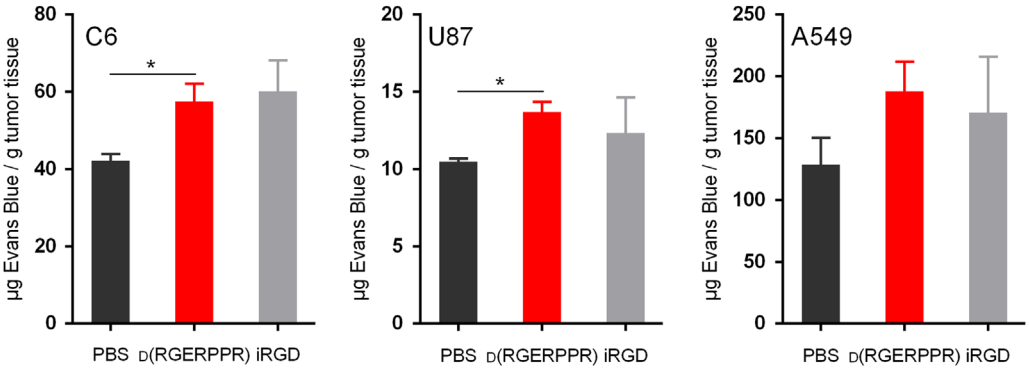

Figure 4 Quantification of tumor-specific entry of Evans blue into different subcutaneous tumor tissues in D(RGERPPR)-injected tumor-bearing mice ($n = 3$).

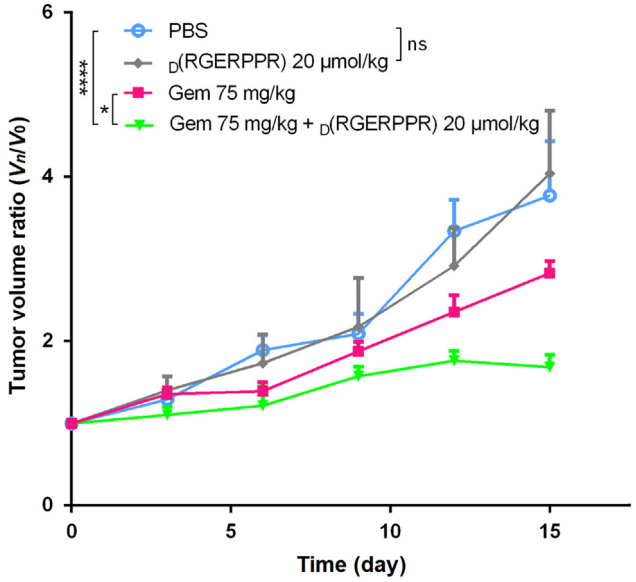

Figure 5 Tumor volume analysis of A549 tumor-bearing nude mice after i.v. injection of PBS, D(RGERPPR), free gemcitabine and gemcitabine combined with D(RGERPPR) ($n = 5$). Administration started on Day 0 and was repeated twice a week for a total of 5 times. Tumor volume was measured every other two days until Day 15. V_n indicates tumor volume at Day n and V_0 indicates tumor volume at Day 0.

in retarding tumor growth, as shown in Fig. 5. The rate of tumor growth in the co-administration group was significantly lower than that of the gemcitabine alone group ($P < 0.05$), with a tumor suppression rate (TSR%) of 55.4%. The enhancement of anti-tumor effects could be attributed to the tumor-penetrating ability of D(RGERPPR), as evidenced above.

4. Discussion

Peptides possess low immunogenicity and high specificity, and are typically easy to synthesize with high quality. Consequently, peptides are widely applied in the treatment of tumors as well as cardiovascular, immune, and hematological diseases, and are also used as recognition molecules for drug delivery systems. However, natural bioactive peptides are susceptible to protease degradation and readily lose bioactivity *in vivo*. In addition, the chains of natural peptides are able to freely rotate and change shapes. Hence, they can completely or partially bind to various receptors, leading to low selectivity. The modification of the structure of bioactive peptides to enhance their stability, specificity, and selectivity has been a research hotspot. Generally, structural transformation of peptides mainly involves the following approaches: 1) substitution of unnatural amino acid, including D-amino acid, *N*-methyl-α-amino acid, β-amino acid, etc.; 2) cyclization of the peptide sequence; 3) isosteric, or not, amide bond replacement between two amino acids; 4) modification of N- or C-terminal ends; and 5) retro-inverso peptides[26]. Among these methods, substitution of D-amino acids has remarkable superiority. First, because of the lack of protease that can degrade D-peptides *in vivo*, substitution of D-amino acid can enhance the biological stability and prolong the plasma half-life[27]. Second, the substitution of D-amino acid also changes the conformation of peptides, which is beneficial to screen the bioactive peptides with high specificity and affinity to target protein.

In 1979, Goodman and Chorev established a retro-inverso peptide method that involved D-amino acids assembled in the reverse order from that in the parent L-sequence[18]. Since the side chain topology of the retro-inverso peptide was similar to that of the parent L-peptide, the retro-inverso peptide might have similar bioactivities as the parent L-peptides. In our previous studies, we selected a CendR peptide (sequence RGERPPR) as the parent L-peptide, and designed its retro-inverso isomer, D(RPPREGR). Our results confirmed that D(RPPREGR) not only exhibited improved cellular uptake efficiency, but also possessed higher tumor-penetrating ability and better biological stability compared to RGERPPR[16].

Since D-peptide shows opposite chirality to the parent L-peptide with the same sequence, the inverso peptide might not have similar bioactivity. However, CendR peptides were a series of specific peptides with R/KXXR/K sequence, of which inverso isomer owned a D(R/KXXR/K) sequence. Since the C-terminal amino acid of the inverso isomer of CendR peptides was also arginine or lysine, we thus speculated that the inverso isomer also had NRP-1 binding activity and tumor-penetrating ability. In this study, we selected RGERPPR as the parent L-peptide and assembled D-amino acid residues in the order of the parent L-peptide sequence to synthesize the inverso peptide D(RGERPPR). As expected, the D(RGERPPR) possessed improved bio-stability (Supplementary Information Fig. S4). And the circular dichroism spectrum results showed that the absorption peak of D(RGERPPR) was enantiomorphous with RGERPPR, indicating that the optical rotation of D(RGERPPR) was opposite to RGERPPR. Surprisingly, the binding affinity of D(RGERPPR) with NRP-1 was significantly higher than that of

RGERPPR. This result could be explained by computer simulation analysis as following: the three DArg residues in $_D$(RGERPPR) fit well with the binding pocket and effectively interact with residues in NRP-1 by hydrogen bond, ion interaction and cation–π interaction. However, in the sequence RGERPPR, only Arg7 at C-terminal could interact well with the residues of NRP-1, and Arg1 and Arg4 formed weak interaction with the backbone of NRP-1. Therefore, $_D$(RGERPPR) possessed stronger binding affinity to NRP-1 than RGERPPR. In the cellular uptake test, the cell uptake amount of $_D$(RGERPPR) was significantly higher than that of FITC-labeled RGERPPR. We also investigated the tumor-penetrating ability by Evans blue test and found that the tumor-penetrating ability of $_D$(RGERPPR) was comparable to iRGD in C6, U87 and A549 tumor-bearing nude mice. Due to its excellent biological activity, $_D$(RGERPPR) could accumulate at tumor tissues and bind to NRP-1 on the surface of tumor cells. By binding NRP-1, $_D$(RGERPPR) enhanced the permeability of tumor blood vessels and tumor tissues, which could facilitate anti-tumor agents to infiltrate into the tumor tissues.

5. Conclusions

By binding NRP-1, the CendR peptides can induce enhanced permeability of tumor blood vessels and tumor tissues. In this study, we selected a CendR peptide (sequence RGERPPR) as the parent L-peptide and synthesized its inverso isomer $_D$(RGERPPR). The results indicated that $_D$(RGERPPR) possessed high binding affinity to NRP-1 and improved tumor cell internalization, which could enhance the permeability of tumor blood vessels and tumor tissues, as well as facilitate anti-tumor agents to penetrate deep into tumor parenchyma. In conclusion, our findings demonstrate that $_D$(RGERPPR) is a potential tumor-penetrating peptide and should be explored in further studies.

Acknowledgments

This work was supported by the National Science Foundation of China (Grant Nos. 81473148 and 81690263) and the Foundation Program of Key Laboratory of Smart Drug Delivery of the Ministry of Education.

Appendix A. Supporting information

Supplementary data associated with this article can be found in the online version at https://doi.org/10.1016/j.apsb.2018.06.006.

References

1. Lu P, Weaver VM, Werb Z. The extracellular matrix: a dynamic niche in cancer progression. *J Cell Biol* 2011;**196**:385–406.
2. Gilkes DM, Semenza GL, Wirtz D. Hypoxia and the extracellular matrix: drivers of tumour metastasis. *Nat Rev Cancer* 2014;**14**:430–9.
3. Baxter LT, Jain RK. Transport of fluid and macromolecules in tumors. I. Role of interstitial pressure and convection. *Microvasc Res* 1989;**37**:77–104.
4. Rofstad EK, Galappathi K, Mathiesen BS. Tumor interstitial fluid pressure—a link between tumor hypoxia, microvascular density, and lymph node metastasis. *Neoplasia* 2014;**16**:586.
5. Mohammadi M, Chen P. Effect of microvascular distribution and its density on interstitial fluid pressure in solid tumors: a computational model. *Microvasc Res* 2015;**101**:26–32.
6. Trédan O, Galmarini CM, Patel K, Tannock IF. Drug resistance and the solid tumor microenvironment. *J Natl Cancer Inst* 2007;**99**:1441–54.
7. Minchinton AI, Tannock IF. Drug penetration in solid tumours. *Nat Rev Cancer* 2006;**6**:583–92.
8. Gatenby RA, Gillies RJ. Why do cancers have high aerobic glycolysis?. *Nat Rev Cancer* 2004;**4**:891–9.
9. Takagi S, Tsuji T, Amagai T, Takamatsu T, Fujisawa H. Specific cell surface labels in the visual centers of *Xenopus laevis* tadpole identified using monoclonal antibodies. *Dev Biol* 1987;**122**:90–100.
10. Kolodkin AL, Levengood DV, Rowe EG, Tai YT, Giger RJ, Ginty DD. Neuropilin is a semaphorin III receptor. *Cell* 1997;**90**:753–62.
11. Oh H, Takagi H, Otani A, Koyama S, Kemmochi S, Uemura A, et al. Selective induction of neuropilin-1 by vascular endothelial growth factor (VEGF): a mechanism contributing to VEGF-induced angiogenesis. *Proc Natl Acad Sci U S A* 2002;**99**:383–8.
12. Miao HQ. Neuropilin-1 is expressed by endothelial and tumor cells as an isoform-specific receptor for vascular endothelial growth factor. *Cell* 1998;**92**:735–45.
13. Teesalu T, Sugahara KN, Kotamraju VR, Ruoslahti E. C-end rule peptides mediate neuropilin-1-dependent cell, vascular, and tissue penetration. *Proc Natl Acad Sci U S A* 2009;**106**:16157–63.
14. Osada H, Tokunaga T, Nishi M, Hatanaka H, Abe Y, Tsugu A, et al. Overexpression of the neuropilin 1 (*NRP1*) gene correlated with poor prognosis in human glioma. *Anticancer Res* 2004;**24**:547–52.
15. Nasarre C, Roth M, Jacob L, Roth L, Koncina E, Thien A, et al. Peptide-based interference of the transmembrane domain of neuropilin-1 inhibits glioma growth *in vivo*. *Oncogene* 2010;**29**:2381–92.
16. Jing W, Yang L, Cao X, Lu W, Wagner E, Xie Z, et al. Retro-inverso CendR peptide-mediated polyethyleneimine for intracranial glioblastoma-targeting gene therapy. *Bioconjugate Chem* 2014;**25**:414–23.
17. Liu M, Li X, Xie Z, Xie C, Zhan C, Hu X, et al. D-peptides as recognition molecules and therapeutic agents. *Chem Rec* 2016;**16**:1772.
18. Goodman M, Chorev M. On the concept of linear modified retro-peptide structures. *Acc Chem Res* 1979;**12**:1–7.
19. Schrödinger. Glide, version 6.6. New York: Schrödinger, LLC, 2013.
20. Halgren TA, Murphy RB, Friesner RA, Beard HS, Frye LL, Pollard WT, et al. Glide: a new approach for rapid, accurate docking and scoring. 2. Enrichment factors in database screening. *J Med Chem* 2004;**47**:1750–9.
21. Friesner RA, Murphy RB, Repasky MP, Frye LL, Greenwood JR, Halgren TA, et al. Extra precision glide: docking and scoring incorporating a model of hydrophobic enclosure for protein-ligand complexes. *J Med Chem* 2006;**49**:6177.
22. Friesner RA, Banks JL, Murphy RB, Halgren TA, Klicic JJ, Mainz DT, et al. Glide: a new approach for rapid, accurate docking and scoring. 1. Method and assessment of docking accuracy. *J Med Chem* 2004;**47**:1739–49.
23. Lim HN, Jang JP, Han JM, Jang JH, Ahn JS, Jung HJ. Antiangiogenic potential of microbial metabolite elaiophylin for targeting tumor angiogenesis. *Molecules* 2018;**23**:563.
24. Murohara T, Horowitz JR, Silver M, Tsurumi Y, Chen D, Sullivan A, et al. Vascular endothelial growth factor/vascular permeability factor enhances vascular permeability *via* nitric oxide and prostacyclin. *Circulation* 1998;**97**:99–107.
25. Sugahara KN, Teesalu T, Karmali PP, Kotamraju VR, Agemy L, Greenwald DR, et al. Coadministration of a tumor-penetrating peptide enhances the efficacy of cancer drugs. *Science* 2010;**328**:1031–5.
26. Vlieghe P, Lisowski V, Martinez J, Khrestchatisky M. Synthetic therapeutic peptides: science and market. *Drug Discov Today* 2010;**15**:40–56.
27. Wei X, Zhan C, Shen Q, Fu W, Xie C, Gao J, et al. A D-peptide ligand of nicotine acetylcholine receptors for brain-targeted drug delivery. *Angew Chem* 2015;**54**:3023–7.